Langmuir

Article

pubs.acs.org/Langmuir

Self-Assembly and Collagen-Stimulating Activity of a Peptide Amphiphile Incorporating a Peptide Sequence from Lumican

Ian W. Hamley,*[,†] Ashkan Dehsorkhi,[†] Valeria Castelletto,[†] Merlin N. M. Walter,[‡] Che J. Connon,[‡] Mehedi Reza,[§] and Janne Ruokolainen[§]

[†]School of Chemistry, Pharmacy and Food Biosciences, University of Reading, Whiteknights, Reading RG6 6AD, United Kingdom

[‡]Institute of Genetic Medicine, Newcastle University, International Centre for Life, Central Parkway, Newcastle upon Tyne NE1 3BZ, United Kingdom

[§]Department of Applied Physics, Aalto University School of Science, P.O. Box 15100, FI-00076 Aalto, Finland

Supporting Information

ABSTRACT: The self-assembly and bioactivity of a peptide amphiphile (PA) incorporating a 13-residue sequence derived from the last 13 amino acids of the C-terminus of lumican, C_{16}-YEALRVANEVTLN, attached to a hexadecyl (C_{16}) lipid chain have been examined. Lumican is a proteoglycan found in many types of tissue and is involved in collagen fibril organization. A critical aggregation concentration (cac) for the PA was determined through pyrene fluorescence measurements. The structure of the aggregates was imaged using electron microscopy, and twisted and curved nanotapes were observed. In situ small-angle X-ray scattering and fiber X-ray diffraction reveal that these tapes contain interdigitated bilayers of the PA molecules. FTIR and circular dichroism spectroscopy and fiber X-ray diffraction indicate that the lumican sequence in the PA adopts a β-sheet secondary structure. Cell assays using human dermal fibroblasts show that below the cac the PA displays good biocompatibility and also stimulates collagen production over a period of 3 weeks, exceeding a 2-fold enhancement for several concentrations. Thus, this PA has promise in future biological applications, in particular, in tissue engineering.

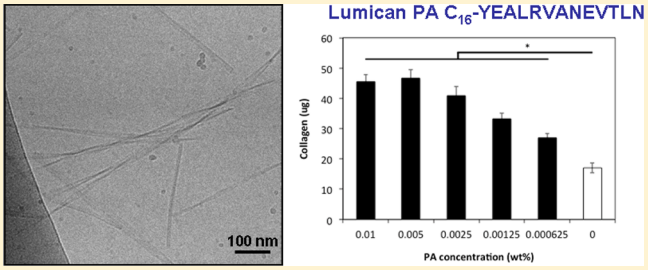

INTRODUCTION

Originally identified as a major keratan-sulfate proteoglycan of the chick cornea, lumican is a small leucine-rich proteoglycan (SLRP) found in a variety of tissues, including skin, bone, articular cartilage, blood vessels, lung, and the invertebral disc.[1] Lumican is composed of 4 major domains: a 16-residue signal protein, a negatively charged N-terminal domain, a tandem leucine-rich repeat region, and a C-terminal domain containing 2 conserved cysteine residues.[2]

Lumican plays a well-characterized role in tissue structure, binding to fibrillar collagens and modulating fibril formation through its leucine-rich repeat region while regulating interfibrilllar spacing through associated glycosaminoglycan (GAG) side chains. Studies suggest that in this capacity it plays an important, if not essential, role in the maintenance of the transparency of the cornea.[3−7] Additionally, lumican has been suggested to influence a range of cell behaviors including adhesion proliferation, migration, tumorigenesis, and differentiation through matrikine interactions.[1,8]

Peptide amphiphiles (PAs) are self-assembling molecules that incorporate bioactive or biomimetic peptide sequences. The conjugation of hydrophilic peptide sequences to hydrophobic lipid chains leads to amphiphilic molecules which have been reported to, most commonly, self-assemble into extended fibrillar nanostructures.[9−16] Other nanostructures including micelles and vesicles can also self-assemble under defined conditions (temperature, pH) depending on the balance of intermolecular interactions.[12,17−19] Peptide amphiphiles have attracted considerable attention recently for applications in biomedicine because the self-assembled nanostructures lead to the presentation of bioactive motifs at high density.[10,11,20,21]

In this article, we investigate the self-assembly of the PA C_{16}-YEALRVANEVTLN which incorporates a 13-residue sequence derived from the last 13 amino acids of the C-terminus of lumican, modified through a C−A substitution (bold) to reduce the loss of function resulting from dimer formation. This sequence has previously been shown to have matrikine properties, e.g., influencing the wound-healing response of the corneal epithelium.[22]

EXPERIMENTAL SECTION

Materials. The PA C_{16}-YEALRVANEVTLN was purchased from CS Bio. The molar mass by ESI-MS was 1730.89 Da (expected 1730.05 Da) as shown in SI Figure 1. The purity was 95.68% as determined by HPLC in TFA (0.1% TFA in H_2O/acetonitrile) as shown in SI Figure 2.

Received: January 8, 2015
Revised: April 1, 2015
Published: April 2, 2015

DOI: 10.1021/acs.langmuir.5b00057
Langmuir 2015, 31, 4490−4495

Pyrene Fluorescence. The critical aggregation concentration was determined via pyrene fluorescence measurements. The fluorescence of pyrene was excited at 335 nm at room temperature, and emission spectra were recorded from 350 to 450 nm using a 10.0 × 5.0 mm^2 quartz cell in a Varian Cary Eclipse spectrofluorimeter. Excitation and emission bandwidths of 2.5 nm were used throughout the experiments. The concentration of pyrene in water was 1.3×10^{-5} M. The same pyrene solution was used to dilute each peptide sample to avoid any dilution effect on pyrene fluorescence due to the addition of subsequent peptide amphiphile aliquots.

Circular Dichroism (CD). In the laboratory, spectra were recorded using a Chirascan spectropolarimeter (Applied Photophysics, U.K.). A sample concentration of 1 wt % dissolved in water was placed in a coverslip cuvette (0.01 mm thick). Spectra are presented with absorbance $A < 2$ at any measured point with a 0.5 nm step, 1 nm bandwidth, and 1 s collection time per step at 20 °C. The post-acquisition smoothing tool in the Chirascan software was used to remove random noise elements from the averaged spectra. A residual plot was generated for each curve in order to verify whether the spectrum has been distorted during the smoothing process. The CD signal from the water was subtracted from the CD data of the peptide solutions.

Fourier Transform Infrared (FTIR) Spectroscopy. Spectra were recorded using a Thermo Scientific Nicolet IS5 or a Nexus FTIR spectrometer, both equipped with a DTGS detector. FTIR data was measured for a 1 wt % solution of C_{16}-YEALRVANEVTLN dissolved in D_2O. Samples were sandwiched between two CaF_2 plate windows (spacer 0.012 or 0.025 mm thick). Spectra were scanned 128 or 168 times over the range of 900−4000 cm^{-1}.

X-ray Diffraction (XRD). X-ray diffraction was performed on stalks prepared by suspending drops of PA solution (1 wt % in water) between the ends of wax-coated capillaries and allowing them to dry. The stalk was mounted vertically onto the four-axis goniometer of a RAXIS IV++ X-ray diffractometer (Rigaku) equipped with a rotating anode generator. The XRD data was collected using a Saturn 992 CCD camera.

Cryo-Transmission Electron Microscopy (Cryo-TEM). Experiments were carried out using a field emission cryo-electron microscope (JEOL JEM-3200FSC) operating at 300 kV. Images were taken using bright-field mode and zero-loss energy filtering (omega type) with a slit at 20 eV. Micrographs were recorded using a Gatan Ultrascan 4000 CCD camera. The specimen temperature was maintained at −187 °C during the imaging. Vitrified specimens were prepared using an automated FEI Vitrobot device using Quantifoil 3.5/1 holey carbon copper grids with a 3.5 μm hole size. Grids were cleaned using a Gatan Solarus 9500 plasma cleaner just prior to use and then transferred into the environmental chamber of an FEI Vitrobot at room temperature and 100% humidity. Thereafter, 3 μL of sample solution at 2 wt % concentration was applied on the grid, blotted once for 1 s, and then vitrified in a 1/1 mixture of liquid ethane and propane at −180 °C. Grids with vitrified sample solutions were maintained in a liquid-nitrogen atmosphere and then cryo-transferred into the microscope.

Small-Angle X-ray Scattering (SAXS). Experiments were performed on beamline B21 at Diamond Light Source, Harwell, U.K. A solution of 1 wt % C_{16}-YEALRVANEVTLN was loaded into a 96-well plate which was then injected via an automated sample exchanger at a slow and very reproducible flux into a quartz capillary (1.8 mm internal diameter). The sample was then placed in front of the X-ray beam. The quartz capillary was enclosed in a vacuum chamber in order to avoid parasitic scattering. After the sample was injected in the capillary and reached the X-ray beam, the flow was stopped during the SAXS data acquisition. B21 operated with a fixed camera length (4 m) and fixed energy (12.4 keV) allowing data collection for $q = 0.015-0.3$ $Å^{-1}$ ($q = (4\pi\sin\theta)/\lambda$, with $\lambda = 1$ Å). The images were captured using a Pilatus 2 M detector. Data processing (background subtraction, radial averaging) was performed using the dedicated beamline software Scatter.

In Vitro Biocompatibility and Bioactivity Assays. Human dermal fibroblasts were maintained for 3 weeks in serum-free DMEM/F12 culture medium (Life Technologies, Paisley, U.K.) supplemented with ascorbic acid, ITS (insulin, transferrin, selenium) (Life Technologies), and antibiotics (Life Technologies), either in the absence or presence of PA at a range of concentrations (1×10^{-2}, 0.5×10^{-2}, 0.25×10^{-2}, 1.25×10^{-3}, and 6.25×10^{-4} wt %), which were obtained by dilution of a 0.1 wt % stock solution. After 3 weeks, the number of viable cells present was assessed by the Alamar Blue assay,[23] which correlates metabolic activity to the reduction of a resazurin sodium salt (Sigma-Aldrich, Dorset, U.K.) to resorufin, quantified via fluorescent emission at 590 nm in response to excitation at 545 nm using a Fluoroskan Ascent (Thermo Scientific, Paisley, U.K.). These cultures were subsequently fixed in ice-cold ethanol and stained with Sirius red/picric acid solution overnight.[24] The bound dye was recovered by agitation in 1 M NaOH, and total collagen was calculated by comparing the absorbance of the resulting samples at 490 nm, read using a Multiskan Ascent (Thermo Scientific), to that of known standard concentrations of collagen.

RESULTS

The critical aggregation concentration (cac) was determined through a pyrene fluorescence assay. The fluorescence vibrational structure of pyrene is sensitive to its environmental hydrophobicity and has been successfully used previously to determine the cac of amphiphilic molecules including surfactants[25,26] and more recently for PAs.[27−31] The cac of C_{16}-YEALRVANEVTLN in water was estimated by observing the fluorescence intensity at the I_1 (λ = 383 nm) peak, which corresponds to the first vibronic band of pyrene. The concentration dependence of I_1 (Figure 1) shows a break at a concentration of cac = (0.03 ± 0.009) wt %. This cac is not detected in a plot of the ratio of the intensity of the first to third pyrene vibronic bands, I_1/I_3 (as shown in SI Figure 3). At higher concentration (above approximately 0.07 wt %) the cloudiness of the solutions prevented reliable fluorescence measurements, and apparent breaks in I_1 and I_1/I_3 are not reliable. The trend in I_1/I_3 as a function of concentration is not that noted for conventional amphiphiles for which I_1/I_3 decreases at the critical micelle concentration, from a typical value of around 1.7−1.8 to a lower value of 1.0−1.2 (e.g., refs 32 and 33). We do not have a detailed explanation for this at present, although one observation is that in contrast to conventional surfactants and amphiphilic polymers, many peptide amphiphiles incorporate aromatic residues (as in the case of the PA studied here) which may influence the fluorescence of pyrene. Nevertheless, we have found from recent studies that I_1 provides a reliable assay for cac values.[30,34] Specifically, in the case in which β-sheet formation occurs

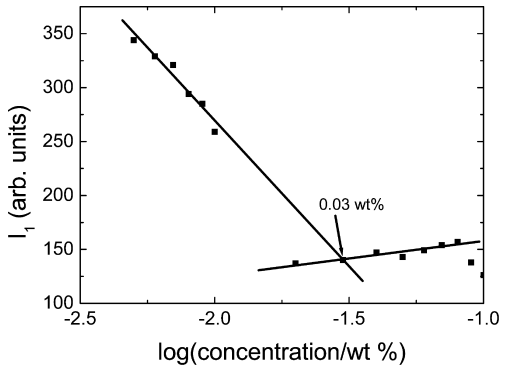

Figure 1. Dependence of the pyrene I_1 fluorescence peak on the concentration of PA, from which the critical aggregation concentration can be obtained, as indicated.

DOI: 10.1021/acs.langmuir.5b00057
Langmuir 2015, 31, 4490−4495

concurrently with hydrophobic collapse upon aggregation, the cac value is consistent[30] with the value obtained from other probe molecules, in particular, Thioflavin T which probes aggregation into amyloid fibrils rather than a change in hydrophobic environment as for pyrene.

Spectroscopic methods were used to examine the secondary structure of the PA well above both of these cac's. Figure 2

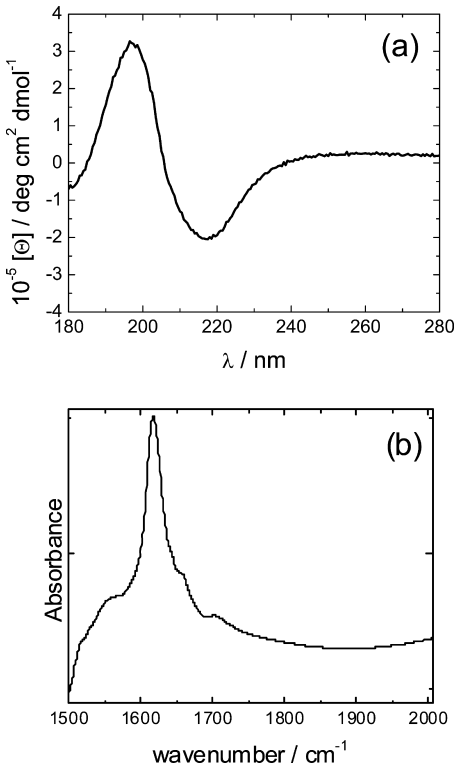

Figure 2. Spectroscopic data obtained from 1 wt % solutions of PA. (a) Circular dichroism spectrum and (b) FTIR spectrum in the amide I′ region.

shows circular dichroism (CD) and FTIR spectra for a 1 wt % aqueous solution of the PA. The CD spectrum (Figure 2a) has a minimum at 216 nm, characteristic of β-sheet secondary structure.[35−37] The FTIR spectrum in the amide I′ region (Figure 2b) supports this assignment, with a strong peak at 1617 cm^{-1}.[38,39] The shoulder peak at 1658 cm^{-1} indicates a small contribution from α-helix secondary structure.[38,39] The peak at 1703 cm^{-1} is assigned to the carbonyl stretch.[29,40−42]

X-ray diffraction was performed on a stalk prepared by drying a 1 wt % solution. The obtained 2D patterns were isotropic, and the data were reduced to 1D intensity profiles as shown in Figure 3. The data contain higher-order peaks from a lamellar structure (d = 20.6 and 10.5 Å), the first order of which was observed by in situ SAXS measurements (vide infra). The profile also features peaks at 4.72 Å (strand separation in the β sheets[19,27,28]) and 3.79 Å (C_α−C_α spacing in a β-sheet structure). The XRD data provide important support concerning the formation of layer structures by the PA, as further probed using SAXS as discussed shortly.

The self-assembled nanostructure of the PA was imaged using cryogenic transmission electron microscopy (cryo-TEM), which is a technique whereby the aqueous phase is vitrified, "trapping" any self-assembled structure and avoiding the need to dry or stain the sample, in contrast to conventional negative-

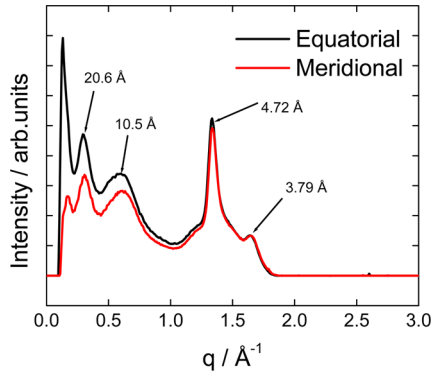

Figure 3. XRD intensity profiles obtained by the integration of a fiber XRD pattern along the two indicated directions.

stain TEM. Figure 4 shows typical images. The morphology is mainly short and straight tapelike structures. Twisting and

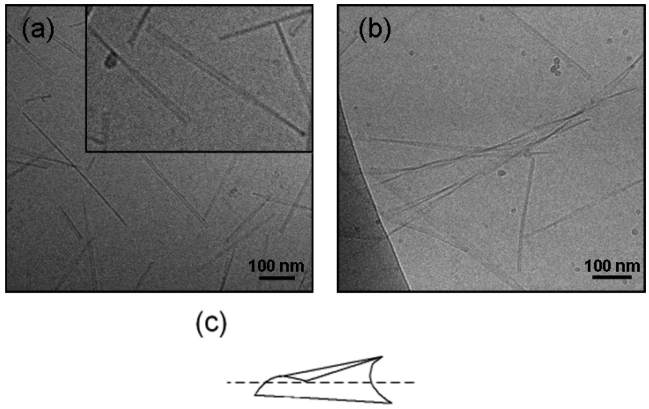

Figure 4. Representative cryo-TEM images obtained from solutions of PA C_{16}-YEALRVANEVTLN. (a) 1 wt % solution, (b) 0.1 wt % solution, and (c) schematic of curved tape, to compare to panel a.

curving of the tapelike structures are observed. In particular, the image for the 1 wt % sample in Figure 4a can be interpreted on the basis of curved tape structures, as sketched in Figure 4c. In contrast, mainly twisted tapes were observed for the 0.1 wt % sample (Figure 4b). The stability of cylindrical vs tapelike fibrillar nanostructures will depend on the relative importance of hydrophobic interactions vs inter- and intrapeptide interactions, in particular, interchain hydrogen bonding which stabilizes β sheets. Tapelike nanostructures would be expected when the "amphiphilicity" predominates whereas fibrils are expected for β-sheet-driven assemblies.[43] The 13-residue peptide sequence in C_{16}-YEALRVANEVTLN is longer than that in most designed PAs studied to date, and it is possible that this PA is on the borderline between lipid-like and amyloid peptide-like self-assembly, i.e., between nanotape and fibril structures.

Cryo-TEM was complemented with in situ small-angle X-ray scattering (SAXS) which provides accurate information on the dimensions of the nanostructures and their internal structure. Figure 5 shows the intensity profile measured for a 1 wt % solution of the PA, along with a model form factor fit. The form factor is that for a lipid bilayer structure, comprising three Gaussian functions to represent the electron density variation across the two headgroups and the dense lipid core.[44] The model and its application to PA bilayer structures have been

DOI: 10.1021/acs.langmuir.5b00057
Langmuir 2015, 31, 4490−4495

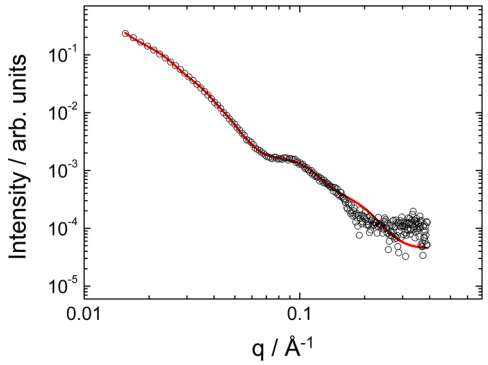

Figure 5. SAXS intensity profile for a 1 wt % solution of the PA (open symbols) along with the fitted form factor model (red line) based on a bilayer structure, as described in the text. For clarity, only every fifth measured data point is shown.

described in detail in our previous papers.[29,45] The fitting was implemented using SASfit software.[46] This form factor provides an excellent fit to the data and confirms that the self-assembled tapes comprise bilayers with a thickness of 51 Å (with a Gaussian polydispersity of 15 Å). The other fit parameters include an overall scaling factor of $s = 2.2 \times 10^{-6}$ as well as the Gaussian width of the outer headgroups (σ_o = 6.0 Å) and of the inner lipid region (σ_i = 5.1 Å) and the corresponding amplitudes ρ_o = 0.00013 and $\rho_i = 5.64 \times 10^{-5}$. The bilayer radius is set to 500 Å, which is much larger than the thickness and so provides only a scaling factor. A flat background, BG = 4.5×10^{-5}, was included in the fit. The value obtained for the layer thickness t indicates that the bilayers comprise highly interdigitated molecules, with some folded peptide residues and/or disorder in the lipid chain, because the extended length of an extended hexadecyl PA containing a 13-residue peptide in a parallel β sheet is expected to be approximately 18 Å (from the C_{16} chain) + 13 × 3.2 Å (from the 13-residue peptide) = 59 Å. The SAXS profile contains, in addition to the form factor profile, a diffuse Bragg peak at $q^* = 0.15$ Å^{-1} corresponding to a bilayer repeat period of 42 Å. The diffuseness of this peak indicates the presence of only a few bilayer repeats, which is consistent with the appearance of the nanotapes observed by cryo-TEM (Figure 4). A sketch of the bilayer structure, consistent with the XRD and SAXS measurements, is provided as Figure 6.

The PA was added to the growth media of human dermal fibroblasts over a range of concentrations, and these cultures were maintained for 3 weeks before assessment for cell number and collagen synthesis. Figure 7 (top) shows that the PA

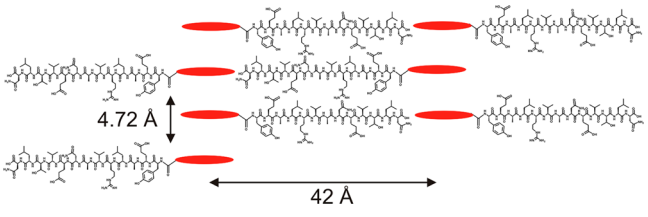

Figure 6. Sketch of the bilayer structure as deduced from XRD and SAXS experiments. The lipid chain is drawn as a red ellipse to indicate that it is not fully extended so that the bilayer spacing (42 Å) is less than the extended molecular length (estimated to be 59 Å). In addition, the peptide β strands may not be fully extended and/or all residues may not be incorporated into the strands.

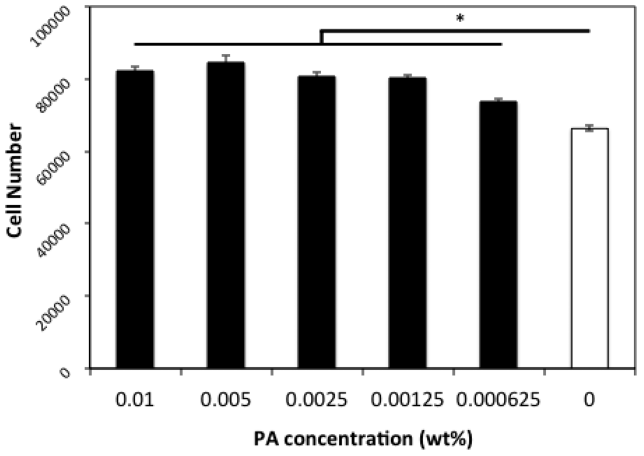

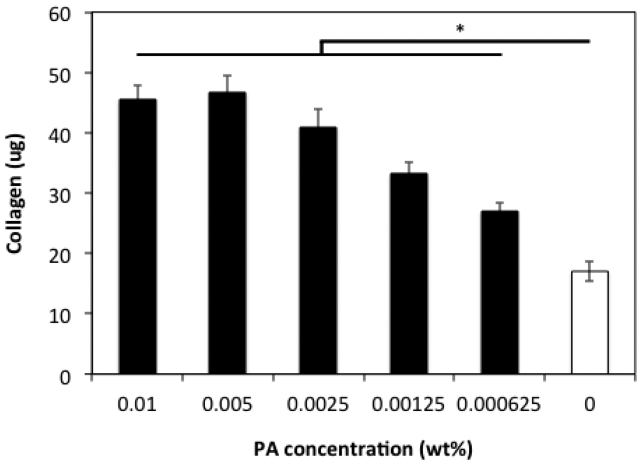

Figure 7. Effect of the PA on HDFa cell number and collagen synthesis over a 3 week culture period. (* denotes $p < 0.05$ by Kruskal Wallace/Tukey's RSD test.)

displayed good biocompatibility, resulting in a modest but significant enhancement of the proliferation of human dermal fibroblasts over 3 weeks in culture. During this period, the presence of PA resulted in a significant and concentration-dependent increase in the amount of collagen produced by these cells, exceeding a 2-fold enhancement at multiple concentrations as shown in Figure 7 (bottom).

■ DISCUSSION

The self-assembly in aqueous solution of a PA incorporating a 13-residue peptide with a sequence from the C-terminal domain of lumican, conjugated to a hexadecyl (palmitoyl) lipid chain, has been investigated using a range of spectroscopic, X-ray scattering, and electron microscopy imaging techniques. A critical aggregation concentration was determined from a pyrene fluorescence assay, and this points to the formation of aggregates with a hydrophobic interior, and possibly also β-sheet order, above a concentration of (0.03 ± 0.009) wt %.

Small-angle X-ray scattering and fiber X-ray diffraction reveal a lamellar structure, which is ascribed to a highly interdigitated bilayer configuration in which the hydrophobic lipid chains are sequestered in the interior of the bilayers. Significant disorder in the lipid chain and/or folding of the PA molecules are implied by the fact that the observed bilayer thickness is smaller than the estimated extended molecular length. However, fiber XRD along with FTIR and CD spectroscopy confirm the β-

DOI: 10.1021/acs.langmuir.5b00057
Langmuir 2015, 31, 4490−4495

sheet secondary structure of the peptide within the PA, indicating that the peptide is in a regular extended conformation. Electron microscopy shows that the self-assemblies comprise twisted tape structures.

The PA shows promising bioactivity because incorporating it into the growth medium of human dermal fibroblasts leads to a modest but detectable proliferation of cells over 3 weeks in culture. Over the same period, a significant and concentration-dependent increase in collagen produced by the cells was observed. Collagen is the major structural protein component of many tissues targeted for biomedical interventions to repair damage, including but not limited to skin, cornea, cartilage, bone, tendons, and ligaments. In each of these tissue types, there is a single fibroblastic or stromal cell population mostly or wholly responsible for the synthesis and maintenance of the collagenous matrix. The reconstitution of damaged collagen by these cells is an essential part of the repair process, with the effectiveness of this often determining the functionality of the resulting material, i.e., scarring/fibrosis vs the full regeneration of new tissue. Similarly, the classical model of tissue repair is often described in terms of phases (i) inflammation, (ii) proliferation, and (iii) maturation. The contribution of this PA to the proliferation of, and collagen synthesis by, human dermal fibroblasts further suggests its potential in the arena of wound repair/tissue regeneration. Tissue engineering methods often seek to combine cells with a suitable scaffold to replicate native tissue. In addition to the synthetic scaffold materials and decellularized donor tissues commonly investigated for this purpose, recently there has been increased interest in the use of cells cultured in vitro to produce a nativelike extracellular matrix for subsequent seeding with tissue-specific cell types to potentially produce "organotypic" engineered tissues.[47] These techniques may benefit greatly from the development of materials that can stimulate the production of extracellular matrix proteins by fibroblasts in vitro and that can, as in the case of PAs, potentially be used as coatings for various surfaces and shapes as suits the requirements of the intended resulting tissue, as well as soluble stimulatory factors.

The data reported in this study does not suggest a specific role for the nanostructure in the effects of the PA upon dermal fibroblasts. We hypothesize that the cells in question respond to the peptide sequence within the amphiphile and that has been previously shown (as an individual peptide fragment rather than as part of a PA) to illicit a migratory response in other cell types.[1,8] The specific effects of the structural state of this PA upon the observed cellular responses are the subject of ongoing investigation.

This PA therefore has strong potential in the development of materials for tissue engineering, specifically for materials to repair damaged extracellular matrixes. This is planned to be the subject of future research.

■ ASSOCIATED CONTENT

Supporting Information

Lipopeptide characterization data and pyrene fluorescence I_1/I_3 assay. This material is available free of charge via the Internet at http://pubs.acs.org.

■ AUTHOR INFORMATION

Notes

The authors declare no competing financial interest.

■ ACKNOWLEDGMENTS

This research was supported by BBSRC grant BB/I008187/1 (to C.J.C. and I.W.H.) and EPSRC grant EP/L020599/1 (to I.W.H.). We are grateful to Katsuaki Inoue and James Doutch for assistance at Diamond (beam-time reference SM10007).

■ REFERENCES

(1) Nikitovic, D.; Katonis, P.; Tsatsakis, A.; Karamanos, N. K.; Tzanakakis, G. N. Lumican, a Small Leucine-rich Proteoglycan. *IUBMB Life* **2008**, *60*, 818−823.

(2) Kobe, B.; Kajava, A. V. The leucine-rich repeat as a protein recognition motif. *Curr. Opin. Struct. Biol.* **2001**, *11*, 725−732.

(3) Chakravarti, S.; Magnuson, T.; Lass, J. H.; Jepsen, K. J.; LaMantia, C.; Carroll, H. Lumican regulates collagen fibril assembly: Skin fragility and corneal opacity in the absence of lumican. *J. Cell Biol.* **1998**, *141*, 1277−1286.

(4) Chakravarti, S.; Petroll, W. M.; Hassell, J. R.; Jester, J. V.; Lass, J. H.; Paul, J.; Birk, D. E. Corneal opacity in lumican-null mice: Defects in collagen fibril structure and packing in the posterior stroma. *Invest. Ophthalmol. Vis. Sci.* **2000**, *41*, 3365−3373.

(5) Quantock, A. J.; Meek, K. M.; Chakravarti, S. An X-ray diffraction investigation of corneal structure in lumican-deficient mice. *Invest. Ophthalmol. Vis. Sci.* **2001**, *42*, 1750−1756.

(6) Beecher, N.; Chakravarti, S.; Joyce, S.; Meek, K. M.; Quantock, A. J. Neonatal development of the corneal stroma in wild-type and lumican-null mice. *Invest. Ophthalmol. Vis. Sci.* **2006**, *47*, 146−150.

(7) Nikitovic, D.; Berdiaki, A.; Zafiropoulos, A.; Katonis, P.; Tsatsakis, A.; Karamanos, N. K.; Tzanakakis, G. N. Lumican expression is positively correlated with the differentiation and negatively with the growth of human osteosarcoma cells. *FEBS J.* **2008**, *275*, 350−361.

(8) Saika, S.; Miyamoto, T.; Tanaka, S.; Tanaka, T.; Ishida, I.; Ohnishi, Y.; Ooshima, A.; Ishiwata, T.; Asano, G.; Chikama, T.; Shiraishi, A.; Liu, C. Y.; Kao, C. W. C.; Kao, W. W. Y. Response of lens epithelial cells to injury: Role of lumican in epithelial-mesenchymal transition. *Invest. Ophthalmol. Vis. Sci.* **2003**, *44*, 2094−2102.

(9) Löwik, D. W. P. M.; Leunissen, E. H. P.; van den Heuvel, M.; Hansen, M. B.; van Hest, J. C. M. Stimulus responsive peptide based materials. *Chem. Soc. Rev.* **2010**, *39*, 3394−3412.

(10) Matson, J. B.; Stupp, S. I. Self-assembling peptide scaffolds for regenerative medicine. *Chem. Commun.* **2012**, *48*, 26−33.

(11) Matson, J. B.; Zha, R. H.; Stupp, S. I. Peptide self-assembly for crafting functional biological materials. *Curr. Opin. Solid State Mater. Sci.* **2011**, *15*, 225−235.

(12) Hamley, I. W. Self-Assembly of Amphiphilic Peptides. *Soft Matter* **2011**, *7*, 4122−4138.

(13) Dehsorkhi, A.; Castelletto, V.; Hamley, I. W. Self-Assembling Amphiphilic Peptides. *J. Pept. Sci.* **2014**, *20*, 453−467.

(14) Trent, A.; Marullo, R.; Lin, B.; Black, M.; Tirrell, M. Structural properties of soluble peptide amphiphile micelles. *Soft Matter* **2011**, *7*, 9572−9582.

(15) Cui, H. G.; Webber, M. J.; Stupp, S. I. Self-Assembly of Peptide Amphiphiles: From Molecules to Nanostructures to Biomaterials. *Pept. Sci.* **2010**, *94*, 1−18.

(16) Lin, Y. A.; Cheetham, A. G.; Zhang, P. C.; Ou, Y. C.; Li, Y. G.; Liu, G. S.; Hermida-Merino, D.; Hamley, I. W.; Cui, H. G. Multiwalled Nanotubes Formed by Catanionic Mixtures of Drug Amphiphiles. *ACS Nano* **2014**, *8*, 12690−12700.

(17) Velichko, Y. S.; Stupp, S. I.; Olvera de la Cruz, M. Molecular simulation study of peptide amphiphile self-assembly. *J. Phys. Chem. B* **2008**, *112*, 2326−2334.

(18) Shimada, T.; Lee, S.; Bates, F. S.; Hotta, A.; Tirrell, M. Wormlike Micelle Formation in Peptide-Lipid Conjugates Driven by Secondary Structure Transformation of the Headgroups. *J. Phys. Chem. B* **2009**, *113*, 13711−13714.

(19) Yu, T.; Lee, O. S.; Schatz, G. C. Steered Molecular Dynamics Studies of the Potential of Mean Force for Peptide Amphiphile Self-

DOI: 10.1021/acs.langmuir.5b00057
Langmuir 2015, 31, 4490−4495

Assembly into Cylindrical Nanofibers. *J. Phys. Chem. A* **2013**, *117*, 7453−7460.
(20) Ustun, S.; Tombuloglu, A.; Kilinc, M.; Guler, M. O.; Teikinay, A. B. Growth and Differentiation of Prechondrogenic Cells on Bioactive Self-Assembled Peptide Nanofibers. *Biomacromolecules* **2012**, *14*, 17−26.
(21) Cheetham, A. G.; Zhang, P. C.; Lin, Y. A.; Lock, L. L.; Cui, H. G. Supramolecular Nanostructures Formed by Anticancer Drug Assembly. *J. Am. Chem. Soc.* **2013**, *135*, 2907−2910.
(22) Yamanaka, O.; Yuan, Y.; Coulson-Thomas, V. J.; Gesteira, T. F.; Call, M. K.; Zhang, Y. J.; Zhang, J. H.; Chang, S. H.; Xie, C. C.; Liu, C. Y.; Saika, S.; Jester, J. V.; Kao, W. W. Y. Lumican Binds ALK5 to Promote Epithelium Wound Healing. *PLoS One* **2013**, 8.
(23) Anoopkumar-Dukie, S.; Carey, J. B.; Conere, T.; O'Sullivan, E.; van Pelt, F. N.; Allshire, A. Resazurin assay of radiation response in cultured cells. *Br. J. Radiol.* **2005**, *78*, 945−947.
(24) Junqueira, L. C. U.; Bignolas, G.; Brentani, R. R. Picrosirius Staining Plus Polarization Microscopy, A Specific Method For Collagen Detection In Tissue-Sections. *Histochem. J.* **1979**, *11*, 447−455.
(25) Kalyanasundaram, K.; Thomas, J. K. Environmental Effects On Vibronic Band Intensities In Pyrene Monomer Fluorescence And Their Application In Studies Of Micellar Systems. *J. Am. Chem. Soc.* **1977**, *99*, 2039−2044.
(26) Winnik, F. M. Photophysics Of Preassociated Pyrenes In Aqueous Polymer-Solutions And In Other Organized Media. *Chem. Rev.* **1993**, *93*, 587−614.
(27) Guler, M. O.; Claussen, R. C.; Stupp, S. I. Encapsulation of pyrene within self-assembled peptide amphiphile nanofibers. *J. Mater. Chem.* **2005**, *15*, 4507−4512.
(28) Sabate, R.; Estelrich, J. Evidence of the existence of micelles in the fibrillogenesis of beta-amyloid peptide. *J. Phys. Chem. B* **2005**, *109*, 11027−11032.
(29) Castelletto, V.; Gouveia, R. J.; Connon, C. J.; Hamley, I. W. New RGD- Peptide Amphiphile mixtures Containing a Negatively Charged Diluent. *Faraday Discuss.* **2013**, *166*, 381−397.
(30) Castelletto, V.; Gouveia, R. J.; Connon, C. J.; Hamley, I. W.; Seitsonen, J.; Nykänen, A.; Ruokolainen, J. Alanine-rich amphiphilic peptide containing the RGD cell adhesion motif: a coating material for human fibroblast attachment and culture. *Biomater. Sci.* **2014**, *2*, 362−369.
(31) Fowler, M.; Siddique, B.; Duhamel, J. Effect of Sequence on the Ionization Behavior of a Series of Amphiphilic Polypeptides. *Langmuir* **2013**, *29*, 4451−4459.
(32) Wilhelm, M.; Zhao, C.-L.; Wang, Y.; Xu, R.; Winnik, M. A.; Mura, J.-L.; Riess, G.; Croucher, M. D. Poly(styrene-ethylene oxide) block copolymer micelle formation in water: A fluorescence probe study. *Macromolecules* **1991**, *24*, 1033−1040.
(33) Johnsson, M.; Hansson, P.; Edwards, K. Spherical micelles and other self-assembled structures in dilute aqeuous mixtures of poly(ethylene glycol) lipids. *J. Phys. Chem. B* **2001**, *105*, 8420−8430.
(34) Hamley, I. W.; Kirkham, S.; Dehsorkhi, A.; Castelletto, V.; Reza, M.; Ruokolainen, J. Toll-like Receptor Agonist Lipopeptides Self-Assemble into Distinct Nanostructures. *Chem. Commun.* **2014**, *50*, 15948−15951.
(35) Hamley, I. W. Peptide fibrillisation. *Angew. Chem.* **2007**, *46*, 8128−8147.
(36) Nordén, B.; Rodger, A.; Dafforn, T. R. *Linear Dichroism and Circular Dichroism: A Textbook on Polarized-Light Spectroscopy*; RSC: Cambridge, 2010.
(37) Woody, R. W. Circular Dichroism of Peptides and Proteins. In *Circular Dichroism: Principles and Applications*; Nakanishi, K., Berova, N., Woody, R. W., Eds.; VCH: New York, 1994; pp 473−496.
(38) Jackson, M.; Mantsch, H. H. The use and misuse of FTIR spectroscopy in the determination of protein structure. *Crit. Rev. Biochem. Mol. Biol.* **1995**, *30*, 95−120.
(39) Stuart, B. *Biological Applications of Infrared Spectroscopy*; Wiley: Chichester, 1997.
(40) Bellamy, L. J. *The Infra-Red Spectra of Complex Molecules*; Chapman and Hall: London, 1975.
(41) Barth, A.; Zscherp, C. What vibrations tell us about proteins. *Q. Rev. Biophys.* **2002**, *35*, 369−430.
(42) Castelletto, V.; Moulton, C. M.; Cheng, G.; Hamley, I. W.; Hicks, M. R.; Rodger, A.; López-Pérez, D. E.; Revilla-López, G.; Alemán, C. Self-Assembly of Fmoc-Tetrapeptides Based on the RGDS Cell Adhesion Motif. *Soft Matter* **2011**, 11405−11415.
(43) Castelletto, V.; Hamley, I. W.; Perez, J.; Abezgauz, L.; Danino, D. Fibrillar superstructure from extended nanotapes formed by a collagen-stimulating peptide. *Chem. Commun.* **2010**, *46*, 9185−9187.
(44) Pabst, G.; Rappolt, M.; Amenitsch, H.; Laggner, P. Structural information from multilamellar liposomes at full hydration: Full q-range fitting with high quality X-ray data. *Phys. Rev. E* **2000**, *62*, 4000−4009.
(45) Castelletto, V.; Cheng, G.; Stain, C.; Connon, C. J.; Hamley, I. W. Self-Assembly of a Peptide Amphiphile Containing L-Carnosine and Its Mixtures with a Multilamellar Vesicle Forming Lipid. *Langmuir* **2012**, *28*, 11599−11608.
(46) http://kur.web.psi.ch/sans1/SANSSoft/sasfit.html. In 2015.
(47) Gouveia, R. J.; Castelletto, V.; Hamley, I. W.; Connon, C. J. New Self-Assembling Multifunctional Templates for the Biofabrication and Controlled Self-Release of Cultured Tissue. *Tissue Eng., Part A* **2015**, DOI: 10.1089/ten.tea.2014.0671.

DOI: 10.1021/acs.langmuir.5b00057
Langmuir 2015, 31, 4490−4495